Multi-view videogrammetry for the estimate of plate sound radiation

Multi-view videogrammetry for the estimate of plate sound radiation

P Gardonio, R Rinaldo, R Del Sal, L Dal Bo, E Turco, A Fusiello
DPIA, Università degli Studi di Udine, Via delle Scienze 206, 33100 Udine, Italy
E-mail: paolo.gardonio@uniud.it

Abstract. This paper explores the possibility of estimating the acoustic pressure field resulting from the vibrations of thin structures using photogrammetric techniques. In particular, the performance of measurement systems using two or more cameras to estimate the displacement of 3D markers placed on the surface of a plate are analyzed by simulation. The projection of the markers on the image plane of each camera is calculated assuming a perfectly calibrated system, in which the errors in the 3D reconstruction of the marker positions are substantially determined by the intrinsic pixellation intrinsic to the measurement process. The acoustic pressure in space is finally calculated, starting from the position of the markers, by means of the Rayleigh integral. The accuracy of the estimate is evaluated by varying the geometry of the cameras setup, their resolution and their number. The results presented show that the estimation of the acoustic radiation is substantially more accurate than the accuracy with which the vibration is estimated. The effect is due to the smoothing operation intrinsically linked to the Rayleigh integration procedure. This study demonstrates the effectiveness of optical systems with multiple, relatively low-cost low-resolution cameras for the measurement of the acoustic pressure field generated by flexural vibrations of distributed structures.

1. Introduction

Measuring the sound radiation of mechanical devices or the transmission of sound through wall structures is an extremely challenging task, requiring rather expensive setups and sophisticated sound detection probes. Acoustic radiation and sound transmission are in fact normally measured both in the vicinity of the structure and in special acoustic rooms. In the first case, the radiated sound field is measured in a few specific points with microphones, or sound level meters [1–3]. Alternatively, certain portions of the radiated sound field can be measured with sound intensity probes, which typically rely on microphones and hot wire transducers to measure the sound pressure and velocity of acoustic particles at a point [1–5]. In more recent schemes, acoustic cameras are employed, which use microphone arrays to measure the noise coming from the vibrating structure, calculating its characteristics with beamforming techniques [6,7]. The measurements carried out in situ, near the vibrating structure, are however often influenced by the impossibility of determining with certainty the operating conditions of the radiant source, by the noise sources external to the structure and by the low repeatability of the measurement configuration [1–3]. In the second case, accurate quantitative measurements of sound radiation by machinery or sound transmission by masonry structures are carried out in complex and expensive test setups, which normally involve rather large reverberant and/or anechoic rooms, equipped with microphones placed in well defined positions, established by

international guidelines [1–5,8]. For example, the sound power radiated by machines is normally measured in large reverberant environments [9]. Alternatively, the transmission of sound through wall structures is measured in reverberant-reverberant or reverberant-anechoic environments, where the tested structure is mounted on an opening in a common wall between the two environments [10].

This paper presents a simulation study on a multi-view videogrammetry setup for the estimate of the sound radiation onto free-field produced by the flexural vibrations of a baffled plate structure excited by an harmonic point force at its fundamental natural frequency. Measuring sound radiation fields is a rather challenging task, both because of their three-dimensional nature and because of their typical frequency content, which, even for low audio frequencies, reaches a few kHz. This study proposes a new approach, where the sound field is reconstructed from the flexural vibration of the structure measured with a multi-view videogrammetry setup. More specifically, the sound field is derived from a finite sum approximation of the Rayleigh integral formula for sound radiation. As shown in Fig. 1, the plate is thus discretised into a regular mesh of radiating elements. The centres of the elements are detailed on the plate by small circular markers, which form a regular grid of measurement points, whose transverse vibrations are measured by the multiple cameras using 3D point tracking. To guarantee convergence to the Rayleigh integral, a rather dense mesh of elements, that is of target points, is considered, whose vibrations can be effectively measured at once by the videocameras. The study assumes the setup is calibrated in such a way as the optic, positioning, etc. parameters of the cameras are taken into account. The cameras are modelled with a classical pinhole model, and the transverse vibration displacement at the plate marker points is reconstructed from triangulation of the views recorded by the whole set of cameras, which, for each marker point, is based on the minimisation of the sum of the squared geometric distances between the measured and the projected image points in the N-cameras. The sound vibration measurement is affected by the errors, primarily due to pixelisation in the photo sensor, introduced by the vibration estimate and by the approximation of the Rayleigh integral. The paper illustrates how the accuracy of the free-field sound radiation estimate varies with respect to: a) the distance of the cameras from the plate; b) the opening angle between pairs of cameras, c) the resolution of the cameras and d) the number of cameras.

The outcome of this study indicates that the vibration measurement errors produced by the image pixelisation in the cameras compensate over the grid of target points so that the estimate of the radiated sound field with the Rayleigh integral formulation results comparatively more accurate than the measured radiation field. This suggests that the proposed method to estimate sound radiation of distributed structures based on flexural vibration measurements with multi-view videogrammmetry has a great potential.

2. Plate sound radiation into free-field

This section introduces the sound radiation model of a thin flat rectangular plate mounted on a rigid baffle. Assuming the classical plate theory [62], the time-harmonic flexural displacement of the plate at position x, y can be described by

$$w\left(x,y,t\right) = \mathrm{Re}\left\{w\left(x,y,\omega\right)e^{j\omega t}\right\}, \tag{1}$$

where

$$w\left(x,y,\omega\right) = \sum_{n=1}^{\infty} w_n\left(x,y,\omega\right) = \sum_{n=1}^{\infty} \phi_n\left(x,y\right) q_n\left(\omega\right). \tag{2}$$

Here, $\phi_n\left(x,y\right)$ and $q_n\left(\omega\right)$ are respectively the shape functions and the complex amplitudes of the flexural natural modes. For a simply supported plate, considering the world Cartesian

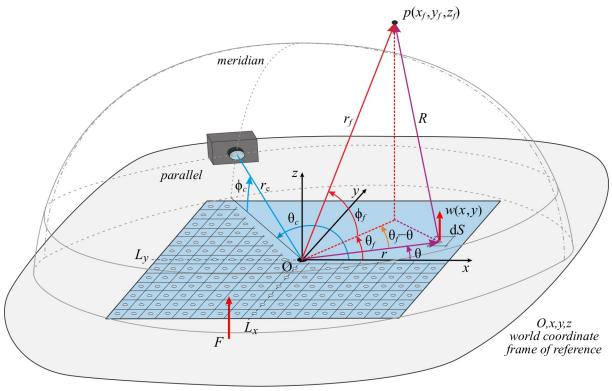

Figure 1. Model problem for the measurement of flexural vibration of a baffled simply supported plate, and of the resulting sound vibration at $p(x_f, y_f, z_f)$.

coordinates, the shape functions are given by [11, 12] (see Fig. 1)

$$\phi_n(x,y) = 2\sin\left(k_{n1}\frac{L_x+2x}{2}\right)\sin\left(k_{n2}\frac{L_y+2y}{2}\right),$$

where, L_x, L_y are the surface dimensions of the plate and $k_{n_1} = \frac{n_1\pi}{L_x}, k_{n_2} = \frac{n_2\pi}{L_y}$ are the bending wavenumbers in x and y directions, being $n_1 = 1, 2, \ldots,$ and $n_2 = 1, 2, \ldots,$ the modal indices for the n-th mode. Also, the complex modal amplitudes are given by

$$q_n(\omega) = \frac{\phi_n(x_F, y_F)F_0}{M[\omega_n^2 + j2\zeta\omega_n\omega - \omega^2]},$$

being $F(x_F, y_F, t) = \mathrm{Re}\left\{F_0 e^{j\omega t}\right\}$ the harmonic transverse point force applied at position x_F, y_F. Table 1 reports the characteristics of the simulated plate.

Table 1. Geometry and physical properties of the plate setup.

Parameter	**Value**
Lateral dimensions	$L_x = 668\,[\mathrm{mm}], L_y = 443\,[\mathrm{mm}]$
Thickness	$h = 19.8\,[\mathrm{mm}]$
Density	$\rho = 7200\ \left[\mathrm{kg/m^3}\right]$
Young's modulus	$E = 14 \times 10^{10}\ \left[\mathrm{N/m^2}\right]$
Poisson ratio	$\nu = 0.31\ [-]$
Modal damping ratio	$\zeta = 0.02\ [-]$
Position of the force	$x_F = 55\ [\mathrm{mm}]\, y_F = 23\ [\mathrm{mm}]$
Grid of markers	$N_x \times N_y = 15 \times 10$
Dimensions of the mesh elements	$d_x = 44.5\ [\mathrm{mm}]\,, d_y = 44.3\ [\mathrm{mm}]$

In general, the response $w(x, y, t)$ at each frequency will be controlled by the modes with natural frequencies ω_n close to the excitation frequency. When the plate is excited at the natural frequency of the first few natural modes, the response can therefore be expressed in terms of the

modal contribution of the resonant mode only, so that

$$w(x,y,t) \simeq \mathrm{Re}\left\{w_n(x,y,\omega)\, e^{j\omega t}\right\} = \mathrm{Re}\left\{w_{n0}(x,y,\omega)\, e^{j(\omega t+\varphi_{n0}(\omega))}\right\}. \tag{3}$$

Similarly, the sound pressure field generated at position (x_f, y_f, z_f) by the time-harmonic flexural vibration of the baffled plate can be expressed as

$$p(x_f,y_f,z_f,t) = \mathrm{Re}\left\{p(x_f,y_f,z_f,\omega)\, e^{j\omega t}\right\},$$

where the complex amplitude $p(x_f, y_f, z_f, \omega)$ is given by the so-called Rayleigh integral [13], which, considering the notation shown in Figure 1 and the approximation in (3), allows to write

$$p(x_f,y_f,z_f,t) \simeq \mathrm{Re}\left\{\frac{j\omega\rho_0}{2\pi}\int_S \frac{w_{n0}(x,y,\omega)\, e^{-jkR}}{R} dS e^{j(\omega t+\varphi_{n0}(\omega))}\right\} \tag{4}$$

$$= \mathrm{Re}\left\{\frac{j\omega\rho_0}{2\pi}\ |q_n(\omega)| \int_S \frac{\phi_n(x,y)\, e^{-jkR}}{R} dS\, e^{j(\omega t+\varphi_{n0}(\omega))}\right\}. \tag{5}$$

Here, $k = \omega/c_0$ is the acoustic wavenumber, where ρ_0 and c_0 are the density and speed of sound for air. Finally, $S = L_x L_y$ is the surface area of the plate and R is the distance between the position $(x, y, 0)$ on the plate and the position in the free-field (x_f, y_f, z_f).

In practice, we can compute Eq. (5) numerically by discretising the plate surface into $N_x N_y$ elements, associated to a set of markers whose displacements are estimated through triangulation, on the basis of their noisy pixel positions in the images acquired by a set of cameras. To obtain a reasonable approximation of the integral, in our simulations we set $N_x \times N_y = 5 \times 10$, as reported in Table 1. Assuming we are observing the pressure field at time instants where the displacement is maximum, the computation of Eq. (5) will be affected by an error, corresponding to the noisy $\hat{w}_{n0}(x, y, \omega)$ estimate obtained with the N cameras. A detailed analysis of the flexural vibration field estimate of a plate structure with multiple cameras is reported in [13].

3. Simulation results

The objective of the simulations presented here is to evaluate the accuracy of the estimation of the acoustic pressure field using various experimental setups, in which parameters such as the distance of the cameras from the plate, their geometric arrangement, the resolution of the cameras and their number are varied. Particular attention is dedicated to the possibility of improving the estimation of the acoustic field obtained by means of low spatial resolution cameras, simply by increasing their number. In fact, [13] shows that the use of multiple cameras significantly improves the vibration estimation, thus allowing a favorable trade-off between spatial and temporal resolution in applications, like that considered here, where the frequencies of interest may require a high camera frame rate. As mentioned, the considered system uses an optical measurement scheme of the plate vibration, and calculates the corresponding acoustic pressure in space using the Rayleigh integral. The sound pressure reference is calculated on the basis of the models presented in Section 2, while its estimate is calculated by approximating the Rayleigh integral with a finite sum of $N_x \times N_y$ contributions, and using the displacement estimate obtained from the images in the cameras as described in [13]. The displacements are affected by errors due to the pixelisation and the process of reconstructing the 3D position of the points.

In the following, the accuracy of the vibration measurement is studied considering the following root mean square error over the $N_t = N_x \times N_y$ grid of plate marker points $P_i = (x_i, y_i)$

$$E_w = \frac{\sqrt{\frac{1}{N}\sum_{i=1}^{N_t}(w_i - \hat{w}_i)^2}}{w_{max}} 100 \quad (\%\ \text{rel.to}\ w_{max}). \tag{6}$$

In this equation, $w_i = w(x_i, y_i, t)$, $\hat{w}_i = \hat{w}(x_i, y_i, t)$ are respectively the actual and estimated transverse displacements and $w_{max} = \max_{i=1,\cdots,N}\{|w(x_i, y_i, t)|\}$ is the maximum actual transverse displacement, at the time instants where the displacement is maximum. Similarly, the accuracy of the sound pressure estimate is analysed considering the root mean square error over the two grids of monitoring points $P_{f,i} = (x_{f,i}, y_{f,i}, z_{f,i})$, located at two grids of $M = M_x \times M_y$ monitoring points arranged on vertical planes XZ and YZ passing through the centre of the plate (see Fig. 2). As a result,

$$E_p = \frac{\sqrt{\frac{1}{M}\sum_{i=1}^{M}(p_i - \hat{p}_i)^2}}{p_{max}} 100 \quad (\% \text{ rel.to } p_{max}). \tag{7}$$

Here $p_i = p(x_{f,i}, y_{f,i}, z_{f,i}, t)$, $\hat{p}_i = \hat{p}(x_{f,i}, y_{f,i}, z_{f,i}, t)$ are respectively the actual and estimated sound pressures and $p_{max} = \max_{i=1,\cdots,M}\{|w(x_{f,i}, y_{f,i}, z_{f,i}, t)|\}$ is the maximum actual acoustic pressure.

The results of the sound radiation estimates will be presented in a standard framework, where each figure shows on the top a table with the values of the parameters kept fixed for the simulation, and then (a) a sketch of the measurement setup with highlighted the parameter being considered; (b) the reference (top maps), best estimate (middle maps) and worst estimate (bottom maps) sound pressure fields on the vertical XZ and YZ planes passing through the centre of the plate; (c) the average error in percent with respect to the maximum radiated sound pressure defined in Eq. (7) (coloured bars).

First, the effect of the distance of a pair cameras from the centre of the plate on the of the radiated sound field is investigated (see Fig. 3). As shown in the top of the figure, the cameras have a low spatial resolution of 320×180 and are positioned at fixed azimuthal θ and elevation ϕ angles and at increasingly larger distances d. The cameras are positioned with a small elevation angle $\phi = 25$ DEG and azimuthal angles $\theta = 60, 120$ DEG such that the two cameras are separated by an opening angle $\alpha = 60$ DEG.

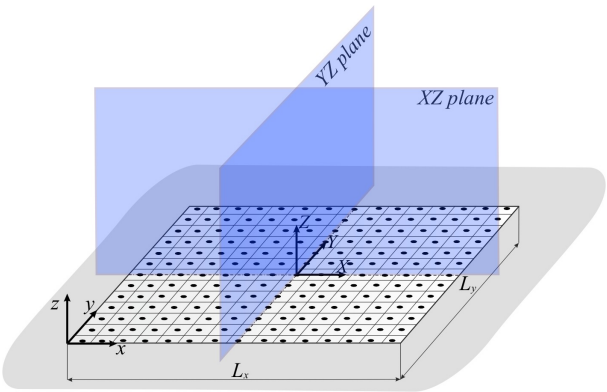

Figure 2. Definition of the planes XZ and YZ on which the sound radiation has been calculated.

Fig. 3 shows that the sound field estimated from the vibration field measured with the cameras reproduces quite accurately the actual radiation field for all camera distances. Indeed, the bar plot (c) reports rather low average errors E_p given respectively by 0.8%, 3.5%, 6.5%, 2%. Interestingly, in this case the average error does not rise monotonically with distance. For instance, when the vibration measurement is made with the cameras at the farthest distance d=1500 mm from the centre of the plate, the mean error of the sound field estimated in the XZ

	Radial distance d (mm)	Elevation angle ϕ (DEG)	Azimuth angle θ (DEG)	Aperture angle α (DEG)	Resolution (pixel)
Values	650 750 1000 1500	25	±30	60	320×180

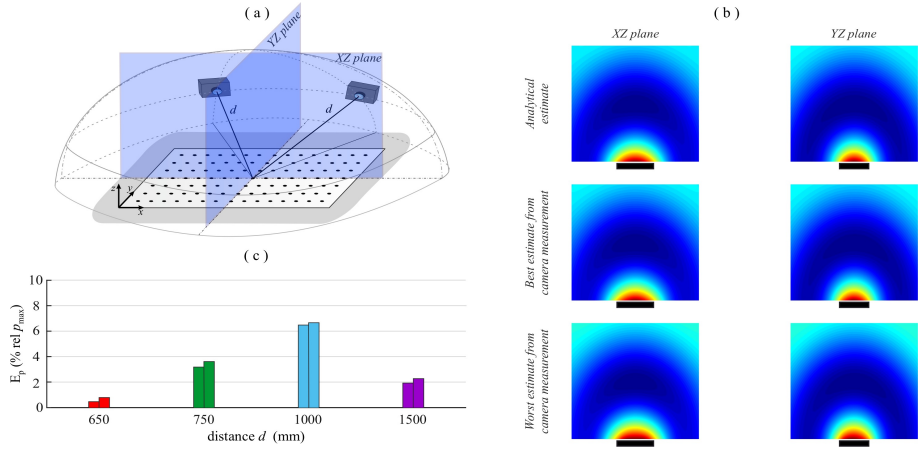

Figure 3. (top) setup summary; (a) distance case study; (b) comparison between ideal (i.e. from analytical model), best and worst case (i.e. from best and worst reconstructed flexural vibration with cameras setup) acoustic fields; (c) bar graph of the mean error.

and YZ planes is about 2%. The average errors of the estimated sound field are comparatively lower than the mean errors of the measured vibration field. For example, when the cameras are placed at d=1500 mm, the average error of the measured vibration field, given by Eq. (6) is about 26% whereas the average error of the estimated sound field is about 2% (more details and results can be found in [13]. This is remarkable outcome, which however suggests that photogrammetry can be suitably used to estimate the sound radiation into free-field generated by flexural vibrations of thin flexible structures.

As a matter of fact, the calculation of the acoustic radiation via the Rayleigh integral equation actually reduces noise, due to smoothing of the errors affecting the estimates of the structure displacement, as highlighted in the following simplified analysis. A rough approximation of Eq. (5) in the far field can be obtained by approximating distances R between the running point on the plate and the far location (x_f, y_f, z_f) as a constant value R_0, since R values become essentially equal to the distance with the centre of the plate. Within such hypothesis, it is easy to derive that the error in the pressure field estimate is proportional to

$$e_p \simeq \sum_{i=1}^{N_p} e_i \Delta S = \frac{L_x L_y}{N_p} \sum_{i=1}^{N_p} e_i,$$

where $N_p = N_x N_y$ is the number of grid points used to calculate the Rayleigh approximation, located at positions (x_i, y_i), ΔS is the area element of the discretised plate surface, and e_i is the vibration error after displacement reconstruction with the optical system, namely

$$\hat{w}_{n0}(x_i, y_i, \omega) = w_{n0}(x_i, y_i, \omega) \; + \; e_i. \tag{8}$$

Indeed, the average implied by Eq. (8) reduces the impact of the vibration estimation error on the pressure field estimation.

Other examples of pressure field estimates are reported in Figs. 4–7, which show the results relative to different camera placements and resolutions. In particular, Fig. 7 reveals a limited dependance of the pressure estimate from the number of cameras, in contrast to the results obtained for the vibration estimates, where E_w monotonically changes from about 12% to 4% when passing from 2 to 12 cameras.

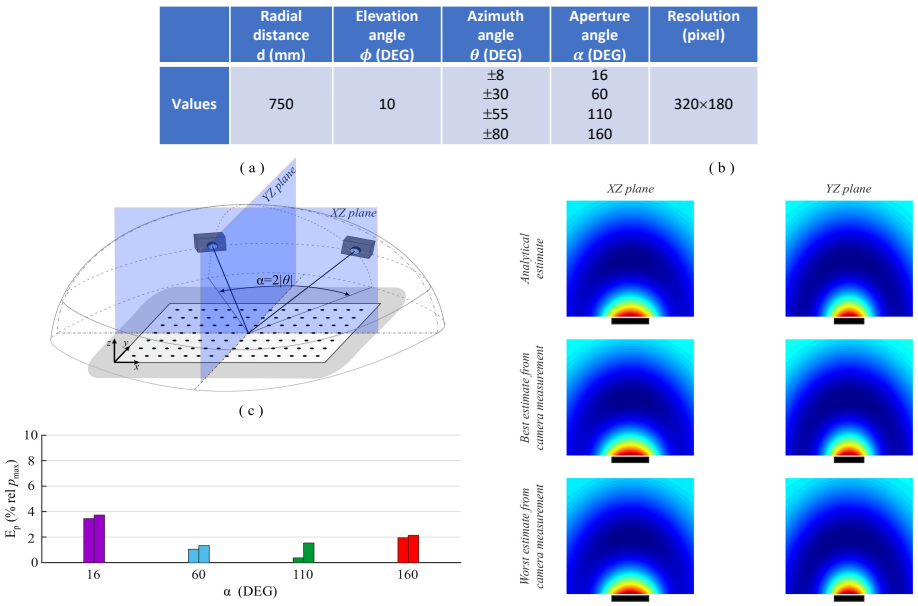

Figure 4. (top) setup summary; (a) opening angle case study; (b) comparison between ideal (i.e. from analytical model), best and worst case (i.e. from best and worst reconstructed flexural vibration with cameras setup) acoustic fields; (c) bar graph of the mean error.

Finally, the colour maps (b) in Fig. 8 show the typical sound radiation fields of the (2,1), (1,2) and (3,1) mode shapes, even when they are reconstructed from the deflection shapes measured with 2 cameras. In this case the bar plots (c) report rather small average errors of the order of 1%. The rather large errors of the order of 20% to 30% reported for the sound fields produced by the deflection shapes resembling the (2,1) and (1,2) modes in the YZ and XZ planes respectively are due to the fact that the (2,1) and (1,2) mode shapes are anti-symmetric with reference to the YZ and XZ planes respectively, so that, due to destructive interference they produce a negligible sound field on these two planes. Consequently, the reconstructed sound fields in these planes are characterised by significant deviations from the theoretical ones and exhibit quite large average errors.

	Radial distance d (mm)	Elevation angle ϕ (DEG)	Azimuth angle θ (DEG)	Aperture angle α (DEG)	Resolution (pixel)
Values	750	5 20 40 60	±90	170 140 100 60	320×180

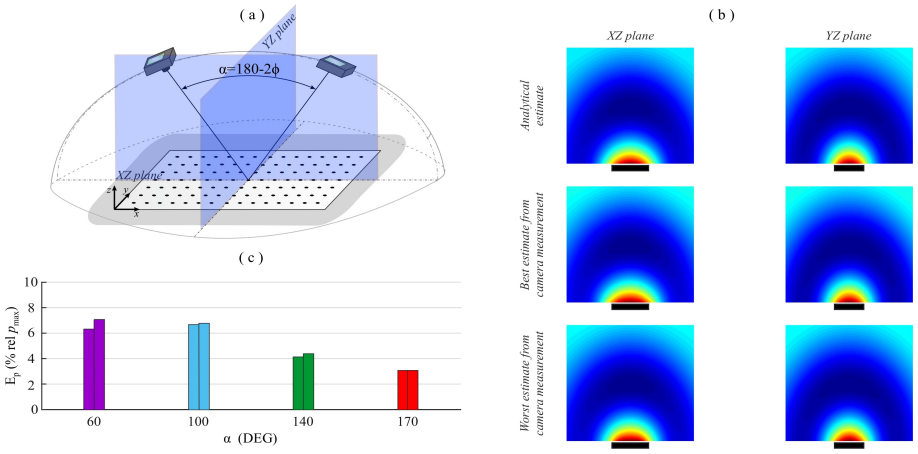

Figure 5. (top) setup summary; (a) opening angle case study; (b) comparison between ideal (i.e. from analytical model), best and worst case (i.e. from best and worst reconstructed flexural vibration with cameras setup) acoustic fields; (c) bar graph of the mean error.

	Radial distance d (mm)	Elevation angle ϕ (DEG)	Azimuth angle θ (DEG)	Aperture angle α (DEG)	Resolution (pixel)
Values	750	25	±30	60	320×180 640×360 1280×720 1920×1080

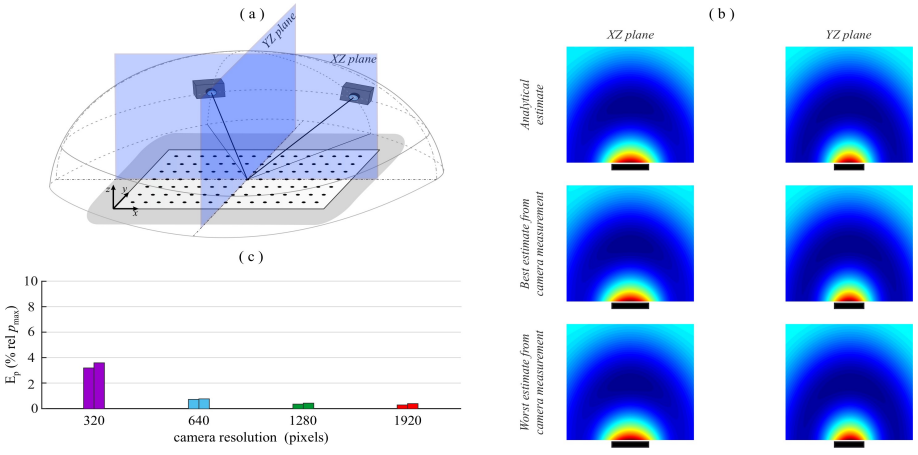

Figure 6. (top) setup summary; (a) resolution case study 3; (b) comparison between ideal (i.e. from analytical model), best and worst case (i.e. from best and worst reconstructed flexural vibration with cameras setup) acoustic fields; (c) bar graph of the mean error.

	Distance d (mm)	Elevation angle ϕ (DEG)	Azimuth angle θ (DEG)	Resolution (pixel)
Values	750	15 15 / 15 15 / 15 / 15 15 / 15 / 15 / 5 15 / 15 / 15 / 5 / 5 15 / 15 / 15 / 5 / 5 / 5	k180+7 k180+ (7 / 27) k180+ (7 / 27 / 0) k180+ (7 / 27 / 0 / 90) k180+ (7 / 27 / 0 / 90 / 47) k180+ (7 / 27 / 0 / 90 / 47 / 60)	320×180

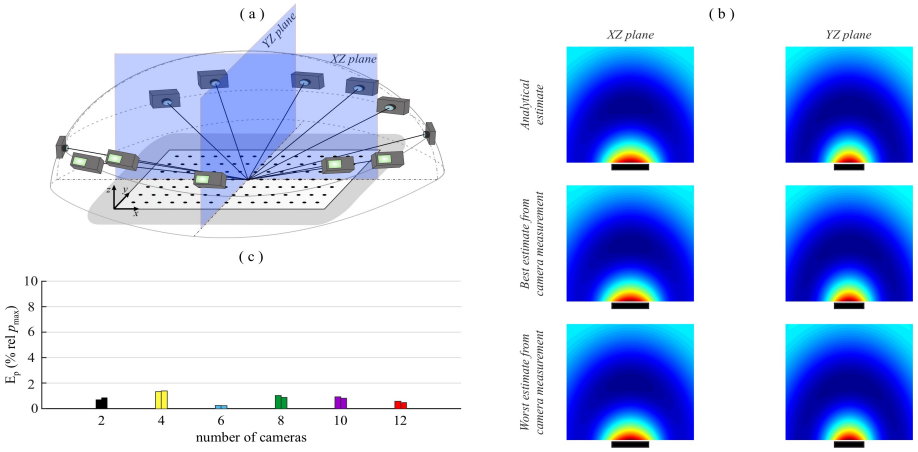

Figure 7. (top) setup summary; (a) multiple cameras case study 4a; (b) comparison between ideal (i.e. from analytical model), best and worst case (i.e. from best and worst reconstructed flexural vibration with cameras setup) acoustic fields; (c) bar graph of the mean error.

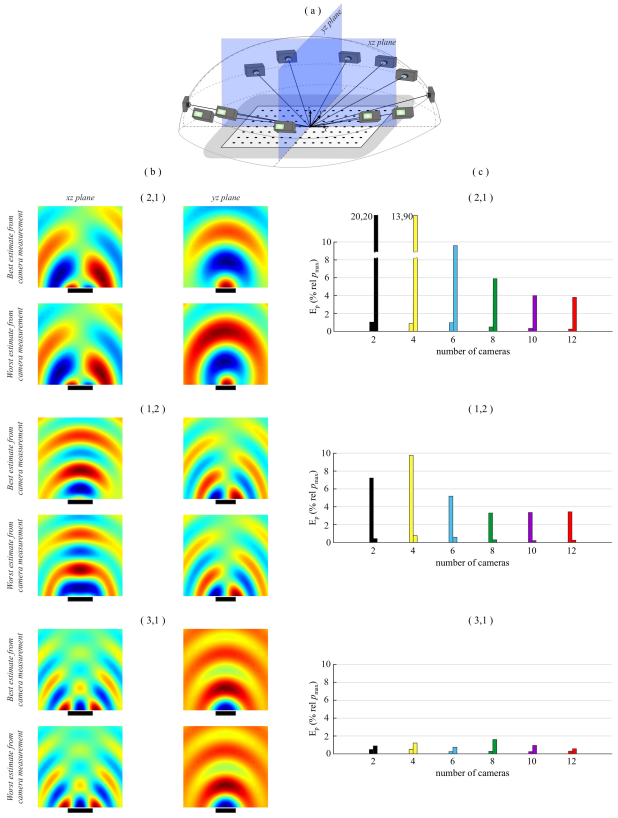

Figure 8. (a) multiple cameras case study 4a; (b) comparison between best and worst reconstructed flexural vibration with cameras setup acoustic fields; (c) histograms of the mean error.

4. Conclusions

In this paper, a comprehensive simulation study has been presented in order to evaluate how the placement, resolution, and number of cameras affect the accuracy of the estimation of the acoustic pressure generated by vibrations of mechanical structures. To this purpose, we considered a simplified simulation arrangement, where errors are generated by pixelisation of images taken from the cameras. The vibration field generated by a plate structure has been considered, where 3D marker positions are reconstructed via triangulation. The pressure field was calculated from the estimated displacement positions obtained by the camera images via the Rayleigh integral. The objective was to assess how the quality of the vibration measurement, with various camera setups, influences the quality of the pressure field estimation. All analyses can be summarised in the following points with respect to the range of parameters considered: 1) the distance of the cameras influences significantly the vibration measurement and to a much less extent the estimate of the sound radiation; 2) the angle of opening between a pair of cameras laid on a circle parallel to and centred on the plate, such that the cameras have a small elevation angle and variable azimuthal angle, does not influence both the vibration measurement and sound radiation estimate; 3) the angle of opening between a pair of cameras laid on a half-circle oriented on a vertical plane passing through the horizontal axis, such that the cameras have a variable elevation angle and fixed azimuthal angle, moderately influence both the vibration measurement and sound radiation estimate; 4) the spatial resolution of the cameras has a significant effect on both the accuracy of the vibration measurement and the accuracy of the sound radiation estimate; 5) setups with more than 2 cameras significantly increase the accuracy of vibration measurements but does not have such an impact on the accuracy of the sound radiation estimate. In conclusion, this study has demonstrated the effectiveness of optical systems with multiple, relatively cheap, low-resolution cameras for the measurement of the acoustic pressure field generated by flexural vibrations of distributed structures.

References

[1] Barron R F 2003 *Industrial Noise Control and Acoustics* (Marcel Dekker Inc., New York)
[2] Bies D A and Hansen C H 2009 *Engineering Noise Control Theory and Practice* (Spon Press, London)
[3] Fahy F 2015 *Measurement of audio-frequency sound in air, in: Fundamentals of Sound and Vibration* (CRC Press)
[4] Fahy F 1995 *Sound Intensity* (CRC Press)
[5] Jacobsen F and de Bree H E 2017 *J. Acoust. Soc. Am.* **66** 1510–1517
[6] Billingsley J and Kinns R 1976 *J. Sound Vib.* **48** 485–510
[7] Merino-Martínez R, Sijtsma P, Snellen M *et al.* 2019 *CEAS Aeronaut. J.* **48** 197–230
[8] Comesaña D F, Steltenpool S, Korbasiewicz M and Tijs E 2015 *Proceedings of EuroNoise 2015* pp 891–895
[9] 2019 *Acoustics - Determination of sound power levels of noise sources* (ISO 3740:2019)
[10] 2000 *Acoustics - Measurement of sound insulation in buildings and of building elements using sound intensity - Part 1: Laboratory measurements; - Part 2: Field measurements; Part 3: Laboratory measurements at low frequencies* (ISO 15186-1:2000)
[11] Reddy J N 2007 *Theory and Analysis of Elastic Plates and Shells* (CRC Press)
[12] Leissa A W 1969 *Vibration of Plates* (NASA Reference Publications, Washington)
[13] Rinaldo R, Gardonio P, Del Sal R, Dal Bo L, Turco E and Fusiello A 2021 *Proceedings of the 14th Intl Conference on Vibration Measurements by Laser and Noncontact Techniques*